Single Source Precursor for PAD-LaMnO$_3$ Thin Films

Ramona Bianca Sonher [1], Richard Attila Varga [2], Mircea Nasui [1], Traian Petrisor Jr [1], Mihai Sebastian Gabor [1], Marin Senila [3], Alessandro Rufoloni [4], Traian Petrisor [1] and Lelia Ciontea [1,*]

[1] Centre for Superconductivity, Spintronics and Surface Science, Physics and Chemistry Department, Technical University of Cluj-Napoca, Str. Memorandumului No. 28, 400028 Cluj-Napoca, Romania; ramona.mos@chem.utcluj.ro (R.B.S.); mircea.nasui@chem.utcluj.ro (M.N.); traian.petrisorjr@phys.utcluj.ro (T.P.J.); mihai.gabor@phys.utcluj.ro (M.S.G.); traian.petrisor@phys.utcluj.ro (T.P.)

[2] Faculty of Chemistry and Chemical Engineering, Babes-Bolyai University, Arany Janos 11, 400028 Cluj-Napoca, Romania; richy@chem.ubbcluj.ro

[3] National Institute for Research and Development of Optoelectronics Bucharest, Research Institute for Analytical Instrumentation, Donath 67, 400028 Cluj-Napoca, Romania; marinsen@yahoo.com

[4] ENEA Frascati Research Centre, 00044 Frascati, Italy; alessandro.rufoloni@enea.it

* Correspondence: lelia.ciontea@chem.utcluj.ro; Tel.: +40-0040-40-1475

check for updates

Abstract: A new lanthanum and manganese ethylenediaminetetraacetate (EDTA) coordination polymer (EDTA^{4-} = [(CH$_2$N)$_2$(CH$_2$-COOH)(CH$_2$COO)$_4$]) was synthesized from La(NO$_3$)$_3$ and Mn(NO$_3$)$_2$ reagents, ethylenediaminetetraacetic acid, and water at room temperature. The structure of the new compound formed, [{La$_2$Mn$_3$(EDTA)$_3$(H$_2$O)$_{11}$}·12H$_2$O]$_n$, was determined by the single crystal X-ray diffraction technique. The synthesis and characterization of the La(III) and Mn(II) coordination complex, characterized by FTIR spectroscopy, thermogravimetry, and differential thermal analysis of the complex, are envisaged. X-ray crystal structure determination indicates that seven- and four-coordinate modes between La(III)/Mn(II) and H$_4$EDTA exist. [{La$_2$Mn$_3$(EDTA)$_3$(H$_2$O)$_{11}$}·12H$_2$O]$_n$ crystallizes in the monoclinic space group *C2* with unit cell parameters of *a* = 16.1227(17) Å, *b* = 14.8049(16) Å, *c* = 14.8736(16) Å, and *β* = 116.107(2)°. Using this precursor, LaMnO$_3$ (LMO) epitaxial thin films were grown by the polymer-assisted deposition (PAD) method on (100)SrTiO$_3$ (STO) single crystalline substrates at a temperature of 900 °C. The LMO crystallized films exhibit a (001)LMO/(001)STO out-of-plane epitaxial relationship and a smooth surface morphology.

Keywords: crystal structure; thin films; EDTA; thermal analysis

1. Introduction

The use of the LaMnO$_3$ (LMO) oxide compound in applications such as magnetic field sensors and electric field devices requires high quality, homogeneous, and uniform surface morphology thin films [1]. Moreover, the LMO thin films represent a very promising buffer layer for the coated conductors' fabrication [2]. LMO has been shown to have the O'-type orthorhombic structure, space group Pbnm, with a = 0.554 nm, b = 0.572 nm, and c = 0.770 nm at room temperature [3]. For a perfect stoichiometry in LMO films, the magnetic ground states are expected to be A-type antiferromagnetic. On the other hand, some authors have experimentally found that stoichiometric LMO thin films grown on SrTiO$_3$ single crystalline substrates present a ferromagnetic behavior [4,5].

It is unanimously accepted that the composition, microstructure, and morphology of the final compound strongly depends on the precursor's nature. In this context, the use of single source

precursors in which preformed bonds exist presents the advantages of obtaining materials with fewer defects and better stoichiometry [6].

Different techniques have been used to prepare LMO thin films such as sol–gel, chemical solution deposition, pulsed laser deposition, and molecular beam epitaxy (MBE) [7,8]. Chemical methods for the chemical deposition of thin film are widespread, very inexpensive, and versatile with respect to the physical deposition techniques. Among the chemical deposition methods, polymer-assisted deposition (PAD) has become efficient to obtain different qualitative thin films [9]. According to this process, a mixture of metal salts and a water-soluble polymer to form a solution with the desired viscosity without gelling was used. The water-based precursor solution is environmentally friendly and exhibits a very good stability in air for a very long period of time (years), an important parameter for the scale-up process [10].

Rare-earth ethylenediaminetetraacetates have been intensively studied for many years due to their applications in different fields, e.g., medicine [11], electronics, or catalysis [12,13]. For example, the lanthanum based ethylenediaminetetraacetate (EDTA) complexes were synthesized with different coordinated anions, which can be used as precursors with application in catalysts [14] and as precursors for the preparation of nanoparticles [15].

Various single crystal structures of EDTA complexes with one or mixed metal coordination have been reported previously. D.S. Liu et al. [16–18] and D.B. Xiong et al. [19] determined the crystal structures of $[Mn_2(EDTA)(H_2O)]_n \cdot nH_2O$ and $\{[La(EDTA)(H_2O)]_2\}_n$ complexes, respectively, obtained by the hydrothermal method.

In this study, the synthesis and characterization of the $[\{La_2Mn_3(EDTA)_3(H_2O)_{11}\} \cdot 12H_2O]_n$ single crystal complex using H_4EDTA as a multidentate ligand at room temperature is reported for the first time. Thermal analysis, infrared spectroscopy, and X-ray diffraction (XRD) analyses are used to characterize the single crystal. Furthermore, in order to demonstrate the potential use of this single source precursor, epitaxial LMO thin films with proper morphological properties were deposited by the PAD technique on $(100)SrTiO_3$ (STO) single crystalline substrates.

2. Materials and Methods

The single crystal was grown by the slow solvent evaporation solution method at room temperature from the $LaMnO_3$ (LMO) precursor solution prepared by the PAD technique. For the synthesis of the LMO precursor solution, the individual metal-polymer aqueous solutions of La^{3+} and Mn^{2+} were synthetized by mixing $La(NO_3)_3 \cdot 6H_2O$ and $Mn(CH_3COO)_2 \cdot 4H_2O$ with ethylenediaminetetraacetic acid (EDTA) in a 1:1 molar ratio. Further details of the precursor solution preparation were described elsewhere [20]. The as-obtained single crystal was characterized by thermogravimetry-differential thermal analysis (TG-DTA) using an SETARAM LabsysEvo thermal analyzer (Lyon, France). Fourier transform infrared (FT-IR) spectroscopy of both single crystal and precursor solutions was performed using a Bruker Tensor 27 FT-IR Spectrometer (Bruker Optik GmbH, Ettlingen, Germany) in attenuated total reflection (ATR) mode. Scanning electron microscopy (SEM) images were investigated using a field emission high resolution SEM (LEO 1525) (LEO Electron Microscopy Inc., Thornwood, NY, USA) provided with an Oxford x-act EDX system. The precursor powder and thin films were investigated by X-ray diffraction measurements performed at room temperature using a Bruker diffractometer operating with Cu K1 radiation (Bruker, Karlsruhe, Germany). Crystallographic data for the structural analysis of the compound were collected on a Bruker SMART APEX system using graphite-monochromated Mo-Kα radiation ($\lambda = 0.71073$ Å). The film surface morphology was investigated using atomic force microscopy (AFM) with a Veeco D3100 atomic force microscope (Veeco Metrology Group, Plainview, NY, USA).

The thermal treatment of the $LaMnO_3$ thin films was performed in two steps in order to avoid porosity at a crystallization temperature of 900 °C in a mixed atmosphere: up to 600 °C with a heating rate of 1 °C/min in a nitrogen atmosphere and up to 900 °C with a heating rate of 5 °C/min in an oxygen atmosphere.

The cell constants of the Complex **1** single crystal are given in Table 1, along with other experimental parameters and relevant information pertaining to the structural solution and refinement (Cambridge Crystallographic Data Center (CCDC) Reference Number 1558664).

Table 1. Crystal data refinement for Complex 1.

Compound	1
Empirical formula	$C_{30}H_{58}La_2Mn_3N_6O_{47}$
Formula weight	1697.46
Temperature (K)	297(2)
Wavelength (Å)	0.71073
Crystal system	Monoclinic
Space group	$C2$
Unit cell dimensions	
a (Å)	16.1227(17)
b (Å)	14.8049(16)
c (Å)	14.8736(16)
α (°)	90
β (°)	116.107(2)
γ (°)	90
Volume (Å^3)	3188.0(6)
Z	2
D_c (mg/cm^3)	1.768
Absorption coefficient (mm^{-1})	2.000
F(000)	1690
Crystal size (mm)	$0.30 \times 0.26 \times 0.23$
θ range for data collection (°)	1.525 to 25.004
Reflections collected	15110
Independent reflections	5597 [R(int) = 0.0365]
Refinement method	Full matrix least-squares on F^2
Data/restraints/parameters	5597/48/461
Goodness-of-fit on F^2	1.020
Final R indices [$I > 2\sigma(I)$]	$R_1 = 0.0319$, $wR_2 = 0.0797$
R indices (all data)	$R_1 = 0.0342$, $wR_2 = 0.0811$
Absolute structure parameter	−0.011(8)
Largest diffraction peak and hole, eA^{-3}	0.891 and −0.353

3. Results and Discussion

3.1. Precursor Characterization

The thermal stability and the decomposition behavior of the single crystal performed in air were investigated by simultaneous TG-DTA analyses (Figure 1a). The general thermal decomposition mechanism of the EDTA complex of the La and Mn single crystal involves three main stages. The first weight loss up to a temperature of 110 °C is attributed to the evaporation of crystallized water molecules. The next mass loss, which occurs between 110 and 200 °C, corresponds to the loss of the coordinated water molecules. A significant mass loss (22%) takes place during the second stage in the temperature range 220–380 °C and corresponds to the decomposition of the EDTA salt, associated with an exothermic peak in the DTA analysis. Above 500 °C, no weight loss in the TG analysis was identified. This means the complete thermal decomposition of the single crystal complex. At 500 °C, after the decomposition of the $[La_2Mn_3(EDTA)_3(H_2O)_{11}]\cdot 12H_2O$ complex, the total residual mass is 68%.
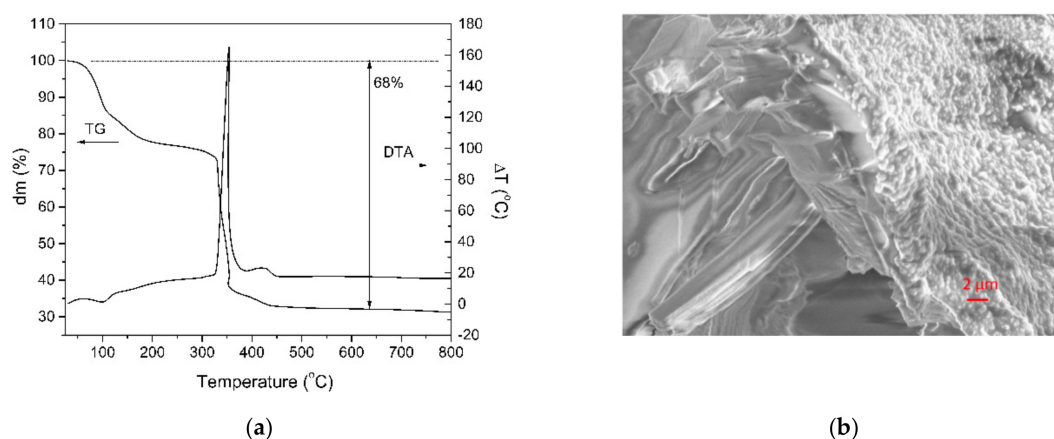
Figure 1. (**a**) TG-DTA analyses of the single crystal complex performed in air and (**b**) the SEM image of the quasi-cleavage fracture of the $[\{La_2Mn_3(EDTA)_3(H_2O)_{11}\}\cdot12H_2O]_n$ crystal at a magnification of 710×.

The $[\{La_2Mn_3(EDTA)_3(H_2O)_{11}\}\cdot12H_2O]_n$ crystal microstructure was investigated by scanning electron microscope. For the investigation, the crystal was in situ fractured under high vacuum in the microscope chamber. The SEM image of the quasi-cleavage fracture surface is shown in the Figure 1b. Except the layer in the vicinity of the surface, the microstructure of the crystal consists of elongated parallelepiped-like crystallites.

In order to investigate the chemical nature of the precursors, FT-IR spectroscopy was used (Figure 2a). The two absorption bands from 1580 and 1407 cm^{-1} were assigned to the asymmetric and symmetric stretching vibrations of the carboxylate group. As can be observed in the FT-IR spectra of the EDTA, the vibration mode from 1683 cm^{-1} is shifted toward lower wavelengths, indicating the complexation of the metal ions. The completely deprotonated EDTA ligand is indicated by the absence of the vibration modes in the range from 1690–1730 cm^{-1}. The Δv value between the $v(COO)_{asym}$ and $v(COO)_{sym}$ of 173 cm^{-1} suggests that the coordination of the carboxylate groups to the metal is chelating mode [21]. This type of coordination is consistent with the results obtained from the single crystal X-ray diffraction data. The presence of peaks below 900 cm^{-1} corresponds to the M-O vibrations.
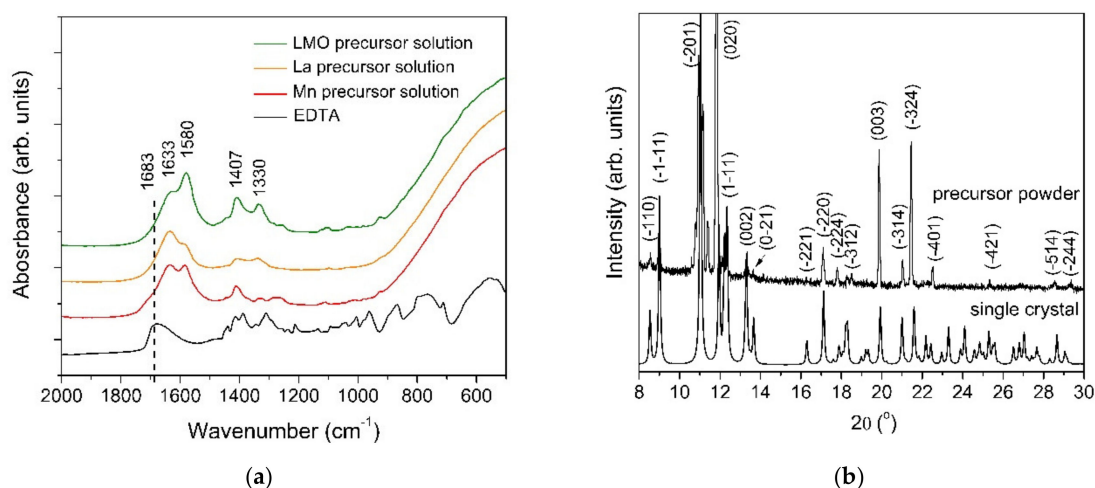
Figure 2. (**a**) FT-IR spectra and (**b**) XRD diffraction pattern of both the precursor powder and single crystal complex.

The experimental XRD patterns of both the precursor powder and the simulated single crystals are depicted in Figure 2b. The DIAMOND software was used to create the drawings. No significant differences between the two XRD patterns at the low angle region were identified, indicating that the two samples have the same crystallographic structure.

3.2. Single Crystal Characterization

The solid state molecular structure, as determined by single crystal X-ray diffraction, is depicted in Figure 3. The crystal structure of Compound **1** reveals that each asymmetric unit contains one La^{III} center, one and half Mn^{II}, and one and half EDTA^{4-} ligand completed by four water molecules coordinated to La, one to one Mn, and a half to the other Mn center, together with six waters as crystallization molecules.
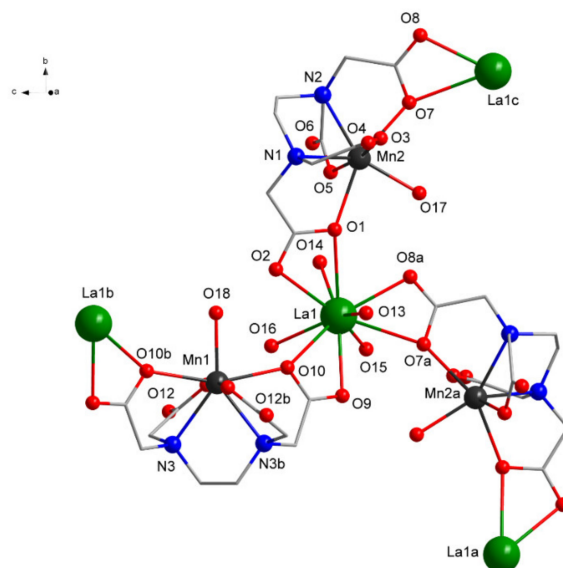
Figure 3. View of the coordination environments of La^{III} and Mn^{II} ions in **1** (H atoms and free water molecules omitted for clarity; symmetry equivalent atoms (3/2 − x, −1/2 + y, −z), (2 − x, y, 1 − z), and (3/2 − x, 1/2 + y, −z) are given by "a", "b", and "c", respectively).

Each La^{III} center is ten-coordinated by three carboxylate O atoms from three chelating EDTA^{4-} ligands and four O atoms coordinating water molecules, while each Mn^{II} is seven-coordinated by four O, two N atoms from one EDTA^{4-}, and one O atom coordinating from the water molecule (Figure 3 and Table 2).

Table 2. Selected bond lengths (Å) and angles (°) for Compound 1.

Atoms 1, 2	d 1,2 (Å) X-ray	d 1,2 (Å) FT-IR	Atoms 1, 2	d 1,2 (Å) X-ray	d 1,2 (Å) FT-IR
La(1)–O(1)	2.747(6)	2.708	Mn(1)–O(10)	2.339(5)	2.325
La(1)–O(2)	2.576(6)	2.565	Mn(1)–O(11)	2.191(6)	2.172
La(1)–O(7a)	2.755(5)	2.733	Mn(1)–O(18)	2.137(10)	2.119
La(1)–O(8a)	2.530(6)	2.545	Mn(1)–O(11b)	2.191(6)	2.172
La(1)–O(9)	2.521(7)	2.551	Mn(1)–O(10b)	2.339(5)	2.325
La(1)–O(10)	2.799(5)	2.711	Mn(1)–N(3)	2.380(6)	2.355
La(1)–O(13)	2.562(5)	2.539	Mn(1)–N(2b)	2.380(6)	2.291
La(1)–O(14)	2.569(6)	2.551			
La(1)–O(15)	2.529(6)	2.544	Mn(2)–O(1)	2.360(6)	2.389
La(1)–O(16)	2.522(6)	2.548	Mn(2)–O(3)	2.187(6)	2.159
			Mn(2)–O(5)	2.200(6)	2.298
			Mn(2)–O(7)	2.347(5)	2.345
			Mn(2)–O(17)	2.136(8)	2.167
			Mn(2)–N(1)	2.374(6)	2.305
			Mn(2)–N(2)	2.338(7)	2.371

Symmetry transformations used to generate equivalent atoms: a, x + 3/2, y + 1/2, −z; b, x + 2, y, −z + 1.

The coordination environment around the La can be described as 16 faced irregular deltahedron, while around Mn, a highly distorted pentagonal bipyramid can be found. The EDTA^{4-} acts as a trimetallic octa-connective chelating ligand forming a bridge between two La^{III} and encapsulating a Mn^{II}.

Table 2 summarizes selected interatomic distances and angles both from the X-ray diffraction measurement and FT-IR analysis using the molecular modeling software)PC Spartan Pro-free Demo 5.0.1., Wavefunction, Inc., Irvine, CA, USA, http://www.wavefun.com). The error in the theoretical prediction is approximately 2%.

In the solid state, the complex forms a two-dimensional layer-type structure (Figure 4), which is strengthened by intramolecular hydrogen bonding between the coordinating water molecules and the O atoms from the ligand (Table 2).
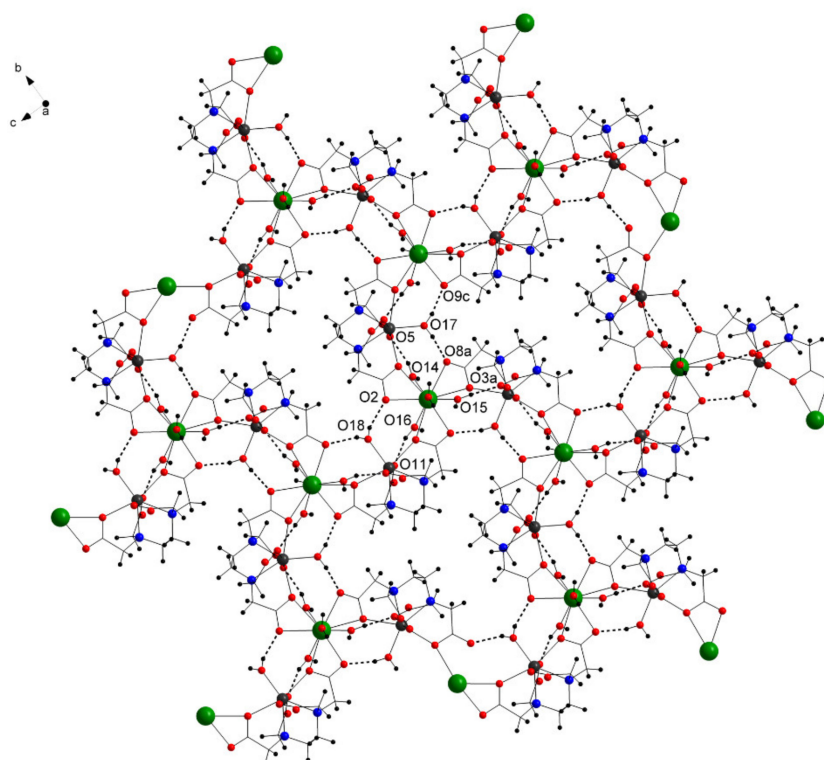
Figure 4. View of the layer framework and the intramolecular hydrogen bonds (dotted lines) along the *a* axis in **1** (free water molecules omitted for clarity).

The layer comprises La$_6$Mn$_6$O$_{12}$ inorganic cycles with a honeycomb-like structure described by the six La^{III} centers (Figure 5). The interior of one hexagonal space is occupied by three Mn centers with their environment.

The layers are connected by several hydrogen bonds between the water molecules coordinated to La from one layer and the carboxyl O from the ligands of another layer, leading to a complex three-dimensional structure (Figure 6). The crystallization water molecules are also involved in inter-layer hydrogen bond interaction (which are not detailed due to the disorder of the water molecules) filling the empty spaces of the three-dimensional structure.
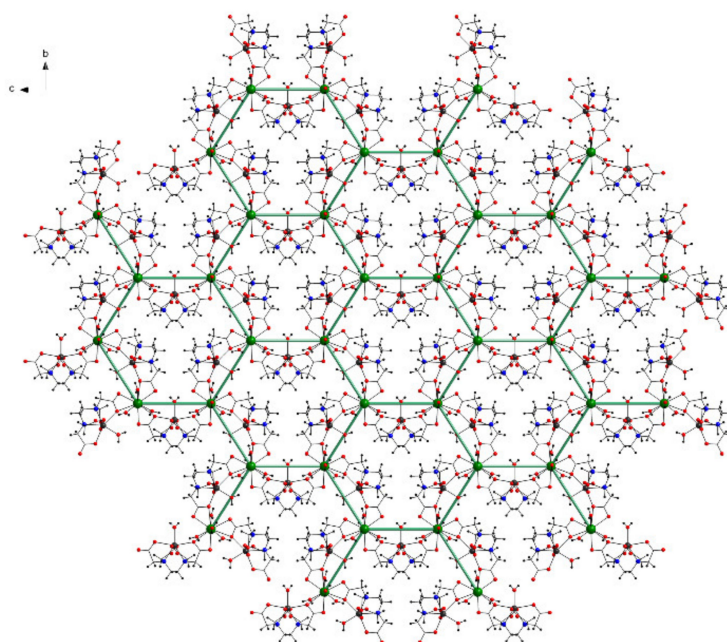
Figure 5. View of the two-dimensional layer with a honeycomb like structure along the a axis in **1** (free water molecules omitted for clarity).
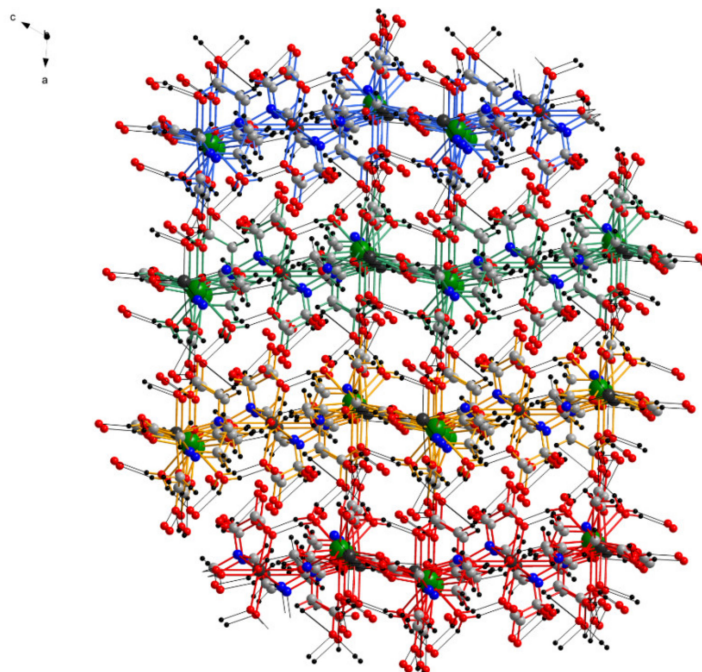
Figure 6. View of the three-dimensional structure in the crystal of 1 along the b axis (layers are drawn with different colors, and hydrogen bonds are shown with black).

The structures were refined with anisotropic thermal parameters. All C-bound H atoms were placed in calculated positions (C–H = 0.97 Å) and treated using a riding model, $U_{iso} = 1.2U_{eq}(C)$. The hydrogen atoms from the coordinated water molecules were found in the difference map and refined with a restrained distance of 0.853(15) Å, 0.848(15) Å, 0.851(15) Å, 0.846(15) Å, 0.849(15) Å, 0.846(15) Å, 0.840(15) Å, 0.845(15) Å, 0.853(15) Å, 0.855(15) Å, and 0.851(15) Å, respectively. The crystallization water molecules were refined without hydrogen atoms, and two of them were disordered and modeled over two positions with site occupancies of 30:70 and 40:60, respectively. The structure was solved using the SHELX-2014 software package [22]. The drawings were created using the DIAMOND program [23].

Table 3 summarizes the crystallographic information and data collection parameters for the single crystal precursor.

Table 3. Hydrogen bonding contacts A–H···B for Complex 1.

D–H···A	Type	d(D–H) (Å)	d(H···A) (Å)	d(D···A) (Å)	<(DHA) (°)
O(14)–H(14D)···O(5)	intra	0.85(4)	1.96(3)	2.786(8)	164(9)
O(15)–H(15D)···O(3a)	intra	0.86(6)	1.96(7)	2.802(9)	167(12)
O(16)–H(16C)···O(11)	intra	0.86(6)	1.90(9)	2.720(9)	161(11)
O(17)–H(17C)···O(8a)	intra	0.84(5)	1.88(7)	2.626(11)	146(14)
O(17)–H(17D)···O(9a)	intra	0.86(5)	1.87(6)	2.712(10)	165(6)
O(18)–H(18D)···O(2)	intra	0.85(6)	2.00(7)	2.765(7)	150(7)
O(13)–H(13C)..O(6d)	inter	0.84(6)	2.05(6)	2.864(11)	162(7)
O(15)–H(15C)..O(4c)	inter	0.85(9)	1.82(9)	2.628(12)	159(8)
O(16)–H(16D)..O(4c)	inter	0.85(7)	1.89(8)	2.691(12)	157(9)

Symmetry transformations used to generate equivalent atoms: a, x + 3/2, y + 1/2, −z; c, 1/2 + x, −1/2 + y, z; d, 1/2 + x, −1/2 + y, z.

3.3. LaMnO₃ Thin Films

In order to evidence the potential of the single source precursors, epitaxial LMO thin films were deposited on (100)SrTiO₃ substrates by the PAD technique. Figure 7a illustrates the AFM image of the LMO thin film thermally treated at 900 °C. The oxide thin film surface investigation showed a homogenous and uniform distribution with a root mean squared roughness (rms) value as low as 7 nm for a 5 × 5 μm scan area. The XRD measurement of the prepared LMO films is presented in the Figure 7b.

(a)

(b)
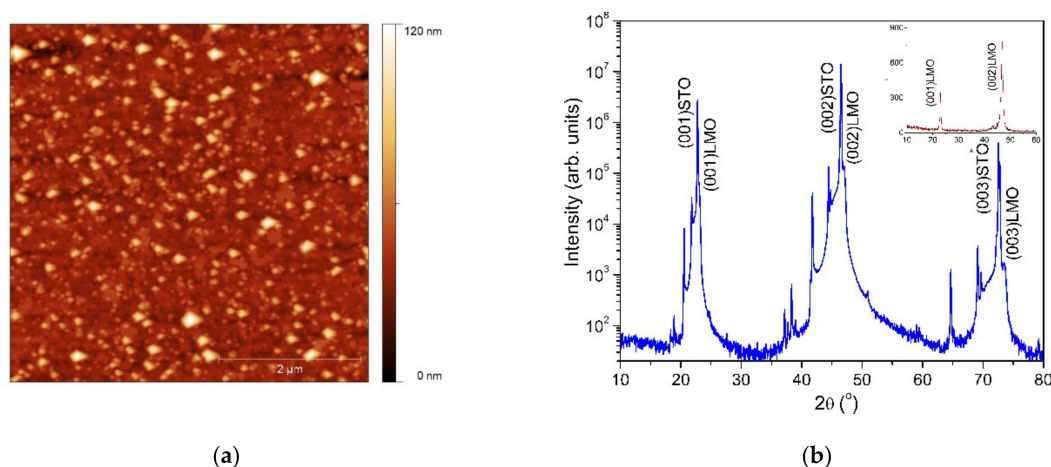
Figure 7. AFM image (**a**) and XRD pattern (**b**) of the LMO film heat treated at 900 °C. Inset: 2θ/ω scan performed with 0.5° offset with respect to the substrate surface normal.

The diffraction pattern presents only (0k0) reflections, indicating that the LMO film is epitaxially grown with a (001)LMO/(001)STO out-of-plane epitaxial relationship. The lattice constant calculated from the (002)LMO diffraction peak is about 3.86 Å, which is close to the stoichiometric LMO (3.88 Å). The mean value of the full-width at half-maximum of the rocking curve is about 0.06°, indicating a good out-of-plane orientation. No secondary phases were detectable in the 2θ/θ scan. This is an indication of the single phase formation of LMO film.

4. Conclusions

A new single crystal of coordination polymer lanthanum and manganese ethylenediaminetetraacetate, [{La₂Mn₃(EDTA)₃(H₂O)₁₁}·12H₂O]ₙ, was obtained for the first

time. The single crystal was characterized by TG-DTA, FT-IR, and XRD measurements, and the molecular structure was determined by X-ray diffraction analyses.

According to the thermal analysis, the $[\{La_2Mn_3(EDTA)_3(H_2O)_{11}\}\cdot 12H_2O]_n$ complex decomposes into three main steps. In the first step, the loss of water molecules occurs (coordinated water). The second step corresponds to the decomposition of the complex. The last decomposition process corresponds to the formation of the final mixed oxide phase. By using single source precursors, the epitaxial growth of LMO films on (100)STO substrates at a temperature of 900 °C was characterized.

References

1. Khanduri, H.; Dimri, M.C.; Vasala, S.; Leinberg, S.; Lohmus, R.; Ashworth, T.V.; Mere, A.; Krustok, J.; Karppinen, M.; Stern, R. Magnetic and structural studies of $LaMnO_3$ thin films prepared by atomic layer deposition. *J. Phys. D Appl. Phys.* **2013**, *46*, 46175003. [CrossRef]
2. Zhu, X.; Lei, H.; Shi, D.; Zhang, L.; Wang, L.; Sun, Y.; Song, W.; Dou, S.; Yang, J.; Gu, H. Chemical Solution Deposition of LaMnO3 Buffer Layers for Coated Conductors. *IEEE Trans. Appl. Supercond.* **2007**, *17*, 3880–3885. [CrossRef]
3. Aruta, C.; Angeloni, M.; Balestrino, G.; Boggio, N.G.; Medaglia, P.G.; Tebano, A. Preparation and characterization of LaMnO3 thin films grown by pulsed laser deposition. *J. Appl. Phys.* **2006**, *100*, 023910. [CrossRef]
4. Gupta, A.; McGuire, T.R.; Duncombe, P.R.; Rupp, M.; Sun, J.Z.; Gallagher, W.J.; Xiao, G. Growth and giant magnetoresistance properties of La-deficient $La_xMnO_{3-\delta}$ ($0.67 \leq x \leq 1$) films. *Appl. Phys. Lett.* **1995**, *67*, 3494. [CrossRef]
5. Vila-Fungueiriño, J.M.; Rivas-Murias, B.; Rodríguez-González, B.; Txoperena, O.; Ciudad, D.; Hueso, L.E.; Lazzari, M.; Rivadulla, F. Room-Temperature Ferromagnetism in Thin Films of $LaMnO_3$ Deposited by a Chemical Method Over Large Areas *ACS Appl. Mat. Interfaces* **2015**, *7*, 5410–5414. [CrossRef] [PubMed]
6. Mlowe, S.; Nyamen, L.D.; Ndifon, P.T.; Malik, M.A.; Raftery, J.; O'Brien, P.; Revaprasadu, N. Aerosol assisted chemical vapor deposition (AACVD) of CdS thin films from heterocyclic cadmium (II) complexes. *Ionrg. Chim. Acta* **2015**, *434*, 181–187. [CrossRef]
7. Shi, D.Q.; Zhu, X.B.; . Kim, J.H.; Lei, H.C.; Wang, L.; Sun, Y.P.; Zeng, R.; Dou, S.X. Chemical solution deposition of LaMnO3-based films for coated conductors. *J. Phys. Conf. Ser.* **2008**, *97*, 012054. [CrossRef]
8. Gadani, K.; Keshvani, M.J.; Dhruv, D.; Boricha, H.; Rathod, K.N.; Prajapati, P.; Joshi, A.D.; Pandya, D.D.; Shah, N.A.; Solanki, P.S. Low field magnetoelectric and magnetotransport properties of sol–gel grown nanostructured $LaMnO_3$ manganites. *J. All. Comp.* **2017**, *719*, 47–57. [CrossRef]
9. Jia, Q.X.; McCleskey, T.M.; Burrell, A.K.; Lin, Y.; Collis, G.E.; Wang, H.; Li, A.D.Q.; Foltyn, S.R. Polymer-assisted deposition of metal-oxide films. *Nat. Mater.* **2004**, *3*, 529. [CrossRef]
10. Mos, R.B.; Petrisor, T., Jr.; Nasui, M.; Calleja, A.; Puig, T.; Ciontea, L.; Petrisor, T. Enhanced structural and morphological properties of Gd-doped CeO_2 thin films obtained by polymer-assisted deposition. *Mater. Lett.* **2014**, *124*, 306–309. [CrossRef]
11. Stavila, V.; Davidovich, R.L.; Gulea, A.; Whitmire, K.H. Bismuth (III) complexes with aminopolycarboxylate and polyaminopolycarboxylate ligands: Chemistry and structure. *Coord. Chem. Rev.* **2006**, *250*, 2782. [CrossRef]
12. Eddaoudi, M.; Kim, J.; Rosi, N.; Vodak, D.; Watcher, J.; O'Keefee, M.; Yaghi, O.M. Systematic Design of Pore Size and Functionality in Isoreticular MOFs and Their Application in Methane Storage. *Science* **2002**, *469*, 132. [CrossRef] [PubMed]

13. Cingolani, A.; Galli, S.; Masciocchi, N.; Pandolfo, L.; Pettinari, C.; Sironi, A. Sorption−Desorption Behavior of Bispyrazolato−Copper(II) 1D Coordination Polymers. *J. Am. Chem. Soc.* **2005**, *127*, 6144. [CrossRef] [PubMed]

14. Guo, Y.-C.; Hou, Y.-H.; Dong, X.; Yang, Y.-C.; Xia, W.-S.; Weng, W.; Zhou, Z.-H. Well-defined lanthanum ethylenediaminetetraacetates as the precursors of catalysts for the oxidative coupling of methane. *Inorg. Chim. Acta* **2015**, *434*, 221–229. [CrossRef]

15. Yi, G.S.; Lu, H.C.; Zhao, S.Y.; Ge, Y.; Yang, W.J.; Chen, D.P.; Guo, L.H. Synthesis, Characterization, and Biological Application of Size-Controlled Nanocrystalline $NaYF_4$:Yb,Er Infrared-to-Visible Up-Conversion Phosphors. *Nano Lett.* **2004**, *4*, 2191. [CrossRef]

16. Liu, D.S.; Sui, Y.; Li, C.H.; Cheng, W.T.; Wang, T.W.; You, X.Z. Synthesis, structure and magnetic properties of a two-dimensional manganese(II) complex with a maximum denticity of ethylenediaminetetraacetic ligand. *Inorg. Chim. Acta* **2011**, *376*, 112–117. [CrossRef]

17. Liu, D.S.; Qiu, Z.J.; Xiao, Y.L.; Dhen, Y.J.; Zhou, Q.; Chen, W.T.; Sui, Y. A novel tetranuclear Pb^{2+} compound based on ethylenediaminetetraacetate and azide mixed-ligands: Synthesis, structure and properties. *J. Solid State Chem.* **2019**, *279*, 120952. [CrossRef]

18. Liu, D.S.; Qiu, Z.J.; Fu, X.; Liu, Y.Z.; Ding, P.; Zhou, Y.X.; Sui, Y. Synthesis, structures and properties of three lead coordination polymers based on ethylenediaminetetraacetate ligand. *J. Solid State Chem.* **2019**, *278*, 120879. [CrossRef]

19. Xiong, D.B.; Chen, H.H.; Yang, X.X.; Zhao, J.T. Hydrothermal synthesis and characterization of a new 1-D polymeric lanthanum ethylenediaminetetraacetate with less metal-aqua coordination: $\{[La(EDTA)(H_2O)]_2\}_n$. *Inorg. Chim. Acta* **2007**, *360*, 1616–1620. [CrossRef]

20. Mos, R.B.; Petrisor, T.; Nasui, M.; Mesaros, A.; Gabor, M.S.; Senila, M.; Ware, E.; Ciontea, L.; Petrisor, T., Jr. Epitaxial $La_{0.7}Sr_{0.3}MnO_3$ nanostructures obtained by polymer-assisted surface decoration (PASD). *Mater. Lett.* **2016**, *171*, 281–284. [CrossRef]

21. Deacon, G.B.; Phillps, R.J. Relationships between the carbon-oxygen stretching frequencies of carboxylato complexes and the type of carboxylate coordination. *Coord. Chem. Rev.* **1980**, *33*, 227–250. [CrossRef]

22. Sheldrik, G.M. A short history of *SHELX*. *Acta Cryst.* **2008**, *A64*, 112–122. [CrossRef] [PubMed]

23. William, T.P. *DIAMOND-Visual Crystal Structure Information System*; Crystal Impact: Bonn, Germany, 2001.